

Chapter 2

Typical Array Geometries and Basic Beam Steering Methods

2.1 Introduction

Any electronic system with an antenna array consists of two or more antenna elements, beam forming network, and a receiver or transmitter. Many different antenna configurations can be utilized as an antenna element in the antenna array: simple dipole, monopole, printed patch design, Yagi antenna, etc. The primary requirement for antennas mounted on/in the car is compact and aesthetic design.

Several locations are considered to use for mounting of the antenna elements on/in the vehicle [1–7, 12]: roof, car window glasses, bumper, or trunk, front panel, side, and rear view mirrors, etc. A typical antenna element mounted on the car roof is a wire or printed on the circuit board monopole. Car glass printed strip antenna elements are proposed for receiving AM/FM radio, TV, and RKE/RSA radio signals, as well as for ITS communication between moving cars or between the vehicle and roadside base station systems [8–11]. Anti-collision antenna arrays [7] are mounted on the car bumper. Typically, antenna array elements are configured as an equally spaced linear design, planar geometry with equal spacing between adjacent elements in each column and row, or antenna elements arranged in a circle with an equal spacing between adjacent antennas. SIMO diversity systems [4, 6] do not require regular arrays with the predetermined spacing between the antenna elements and can use distributed elements with an inter-element spacing more than operating wavelength. Generally, inter-element spacing has to be chosen so to ensure low-level correlation between signals received by adjacent antenna element channels. According to the theoretical results, the low correlation coefficient is obtained for inter-element spacing more than half wavelength; however, experimental measurements show that this distance can be less [13]. Therefore, both compact antenna arrays and distributed multi-element antenna systems are good candidates for automotive car applications.

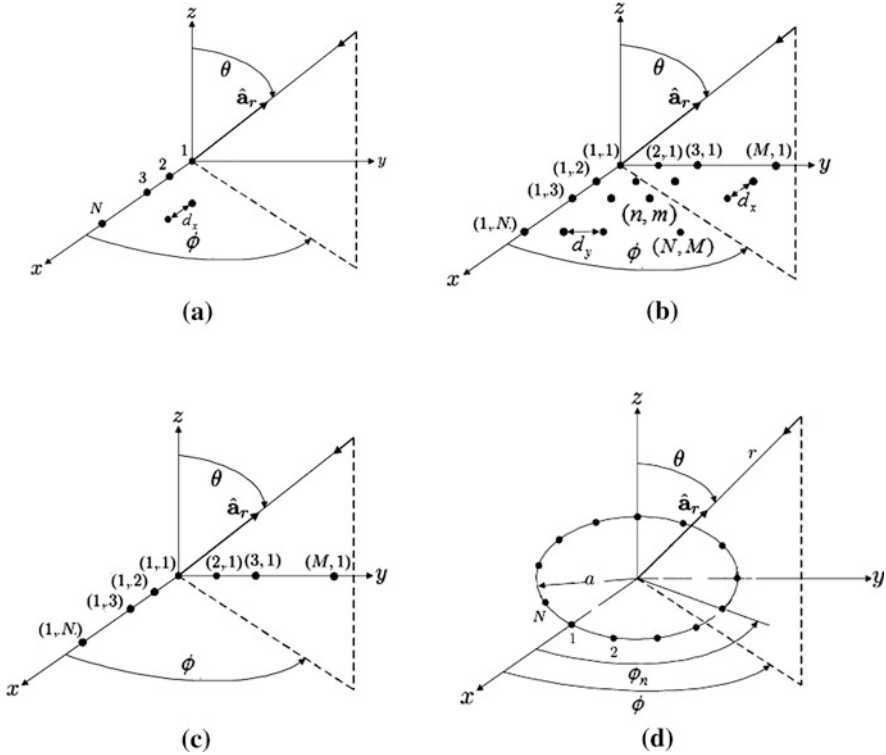


Fig. 2.1 Spherical coordinate system: **a** Linear array; **b** Planar array; **c** Mills cross array; **d** Circular array

2.2 Linear Array Factor for Equally Spaced Elements

The array factor of linear array with equally spaced N isotropic radiating elements placed along horizontal axis x as a function of the angles θ and ϕ in a spherical coordinate system shown in Fig. 2.1a can be expressed by simple formula

$$AF_{\text{linear}}(\theta, \phi) = \sum_{n=1}^N I_n \cdot e^{j(\delta_n + k \cdot d \cdot n \cdot \sin \theta)} \quad (2.1)$$

where I_n and δ_n ($n = 1, 2 \dots N$) are the amplitude and phase excitation of n th array element, d = distance between two adjacent elements, and wave number $k = 2 \cdot \pi / \lambda$ (λ =wavelength).

Values I_n and δ_n are determined by specific design of beam, forming network. Typically, the array factor is expressed by an absolute value (2.1) normalized to its maximum and is plotted in dB scale.

$$|AF_{\text{linear}}^{\text{norm}}(\theta, \phi)| = \frac{|AF_{\text{linear}}(\theta, \phi)|}{\max\{|AF_{\text{linear}}(\theta, \phi)|\}} \quad (2.2)$$

For the uniform amplitude and equal phase distributions ($I_n = I$ and $\delta_n = \delta$, $n = 1, 2, \dots, N$) normalized array factor is given by

$$|AF_{\text{linear}}^{\text{norm}}(\theta, \phi)| = \frac{1}{N} \cdot \left| \frac{\sin\left(\frac{N}{2} \cdot k \cdot d \cdot \sin \theta\right)}{\sin\left(\frac{k \cdot d \cdot \sin \theta}{2}\right)} \right| \quad (2.3)$$

It is seen that the linear factor (2.3) does not depend on ϕ value and has a maximum equal to 1 for the angle direction $\theta = 0$. As we can see, function (2.3) also has maximum value for the following angle directions (grating lobe angle directions)

$$\theta_r = \pm \arcsin\left(\frac{\lambda \cdot r}{d}\right); \quad r = 1, 2, \dots \quad (2.4)$$

If the distance between the adjacent elements is equal or less than the wavelength λ , linear antenna array has only one beam peak within the visible observation angle region (-90° – 90°). When $d > \lambda$ the unwanted beam peak (grating lobe) occurs in the real angle range of -90° – 90° . Therefore, observation angle range dictates the value of the maximum element spacing to avoid the occurrence of the grating lobe. For example, if the observation angle occurs in the range -30° and 30° array element spacing can be chosen as $2 \times \lambda$. As it follows from the formula (2.3), the value of the maximum sidelobe (with respect to the main beam peak) for the array with uniform amplitude distribution is about -13.1 dB, and the angle direction of this lobe can be estimated from the following expression

$$\theta_{\text{max lobe}} = \pm \arcsin\left(\frac{3}{2} \cdot \frac{1}{N} \cdot \frac{\lambda}{d}\right) \quad (2.5)$$

Figure 2.2 shows simulation example results for the normalized linear array factor with different element numbers. All diagrams are obtained for uniform amplitude distribution and normalized to the main lobe value, (normal to the array (direction z) corresponds to the angle 0°) Figs. 2.2a–d are obtained for inter-element spacing equal half wavelength and Fig. 2.2e–h demonstrate the array factor for inter-element spacing equal to one wavelength. As we can see, one wave spacing generates grating lobes with a magnitude equal main lobe value. Values for the maximum side lobes are around -13 dB as it follows from the expression (2.3). The beamwidth of the main lobe between two adjacent nulls is about

$$\Delta\theta_{\text{main}} \approx \frac{2 \cdot \lambda}{d \cdot N} \quad (2.6)$$

The directivity of the broadside linear array factor toward the normal to the array with uniform amplitude and phase distribution is given by [15]

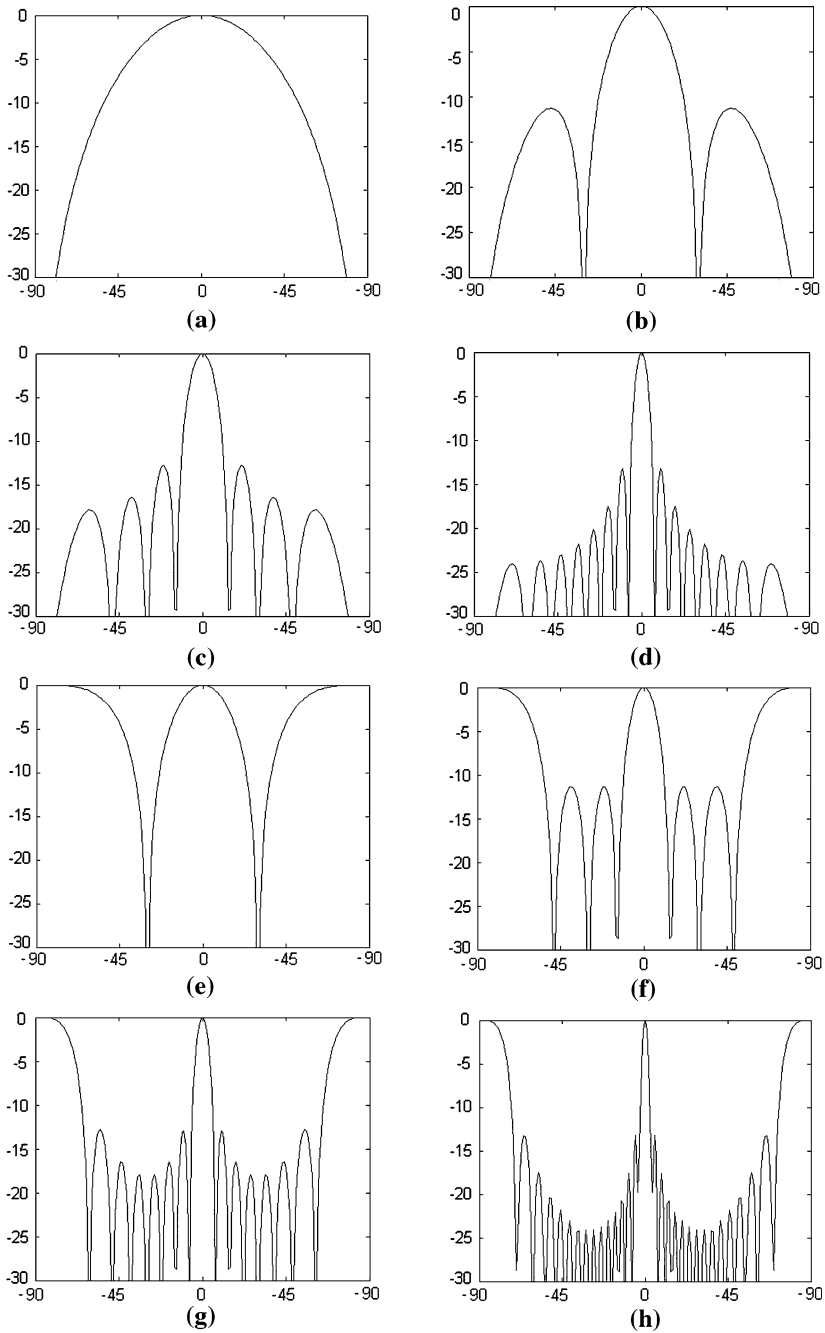


Fig. 2.2 Linear array factor. **a** Two element array, spacing $\lambda/2$; **b** Four element array, spacing $\lambda/2$; **c** Eight element array, spacing $\lambda/2$; **d** Sixteen element array, spacing $\lambda/2$; **e** Two element array, spacing λ ; **f** Four element array, spacing λ ; **g** Eight element array, spacing λ ; **h** Sixteen element array, spacing λ

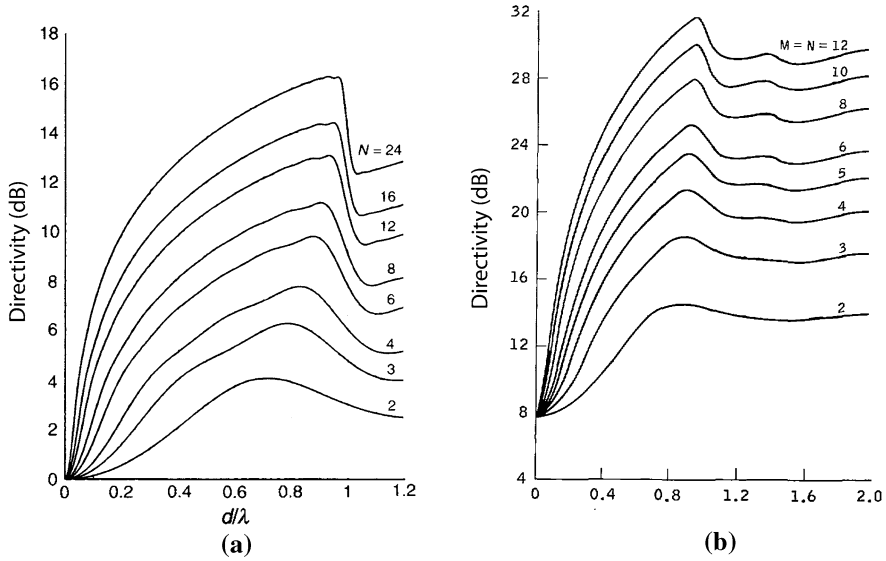


Fig. 2.3 Directivity as a function of the element spacing: **a** Linear array factor; **b** Planar array factor

$$D_{\text{linear}} = \frac{N^2}{N + 2 \cdot \sum_{n=1}^{N-1} \frac{(N-n) \cdot \sin(n \cdot k \cdot d)}{n \cdot k \cdot d}} \quad (2.7)$$

For half wave inter-element spacing, directivity D_{linear} is equal to N . Figure 2.3a shows calculated directivity values as a function of element spacing for different numbers of isotropic elements. It is seen that the directivity graph drops at the appearance of the first grating lobe.

Arrays with feed networks shown in Fig. 1.7c, d produce non-uniform amplitude distribution, which reduces sidelobe level and, therefore, protects the receiving system from interference signals. For example, the maximum sidelobe level can be reduced from -13 dB up to -17 dB (relatively to the main beam peak) if the currents I_n at the edge array elements are about 0.5 from the maximum value at the central array elements and up to -21 to -40 dB for the edge antenna array element currents equal to 0. The amplitude tapering for the feed network shown in Fig. 1.7c or d can be controlled by the distance between the feed antenna and the array plane or by variation of the feed antenna radiation pattern. Non-uniform amplitude distribution across the array can also be realized with parallel, series, or parallel-series networks [16–18] shown in Fig. 1.5. For example, the reference paper [16] describes six element array with series fed network, which provides amplitude distribution with sidelobe level of about -20 dB. However, the amplitude tapering produces the broadening of the main beam and reduced antenna gain. The broadside directivity of the linear array factor with amplitude distribution I_n and equal phases for all elements is given by [19, 20].

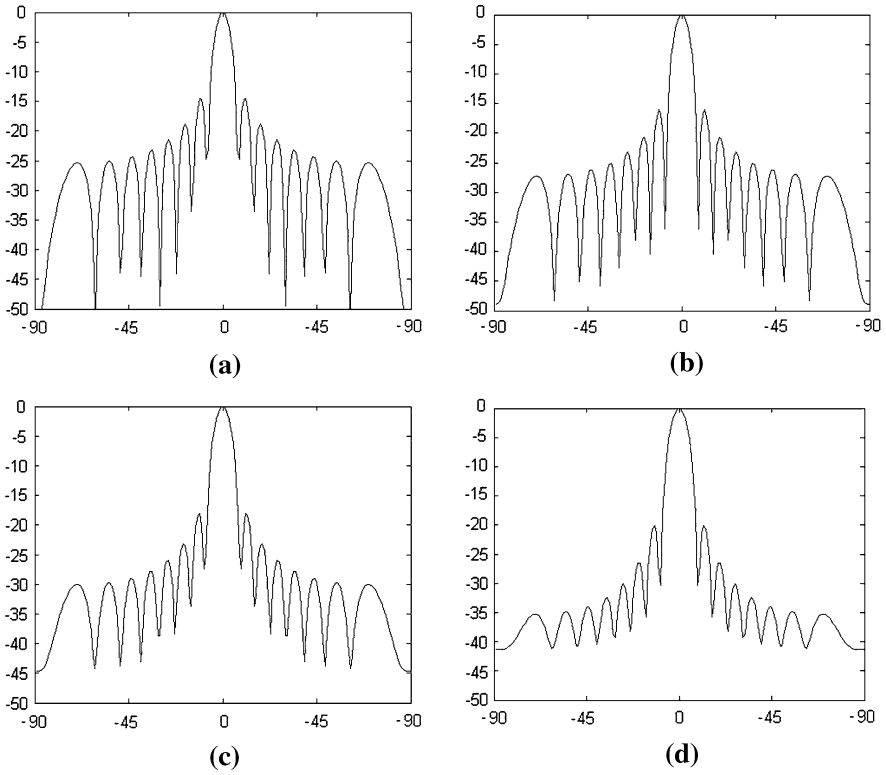


Fig. 2.4 Linear array factor, eight elements, element spacing $\lambda/2$: **a** Uniform amplitude distribution ($\gamma = 0$); **b** $\gamma = 0.4$; **c** $\gamma = 0.6$; **d** $\gamma = 0.8$

Table 2.1 Aperture (taper) efficiency

| N | 16 | 8 | 4 |
|-------------------------------------|-------|-------|-------|
| $\eta_{\text{taper}}(\gamma = 0.2)$ | 0.995 | 0.99 | 0.99 |
| $\eta_{\text{taper}}(\gamma = 0.4)$ | 0.976 | 0.968 | 0.95 |
| $\eta_{\text{taper}}(\gamma = 0.6)$ | 0.936 | 0.916 | 0.862 |
| $\eta_{\text{taper}}(\gamma = 0.8)$ | 0.87 | 0.828 | 0.709 |

$$D_{\text{linear}}^{\text{taper}} = \frac{\left(\sum_{n=1}^N I_n \right)^2}{\sum_{n=1}^N \sum_{m=1}^N I_n \cdot I_m \cdot \frac{\sin((n-m) \cdot k \cdot d)}{(n-m) \cdot k \cdot d}} \quad (2.8)$$

The ratio $\eta_{\text{taper}} = \frac{D_{\text{linear}}^{\text{taper}}}{D_{\text{linear}}}$, named as excitation (taper, or aperture) efficiency, determines the directivity loss due to the tapering amplitude from the center array

to the edges. When the distance between the array elements is equal to half of the wavelength, η_{taper} is given by

$$\eta_{\text{taper}} = \frac{\left(\sum_{n=1}^N I_n \right)^2}{N \cdot \sum I_n^2} \quad (2.9)$$

For a uniform amplitude distribution, excitation efficiency is equal to 1. If the first sidelobe level of about -18 dB η_{taper} is around 0.95 (-0.22 dB) [20], for first sidelobe value of -23 dB $\eta_{\text{taper}} = 0.81$ (-0.92 dB), and for first sidelobe level equal to -31.5 dB $\eta_{\text{taper}} = 0.67$ (-1.7 dB). Figure 2.4 shows simulation result examples of the linear array factor with the number of elements $N = 8$, inter-element spacing equal to half of the wavelength, and different non-uniform amplitude distribution functions (normal to the array (direction z) corresponds to the angle 0°).

$$I_n = 1 - \gamma \cdot \left(\frac{n - N/2 - 0.5}{N/2 - 0.5} \right)^2 \quad (2.10)$$

Amplitude vales (2.10) are symmetrically equal, i.e., $I_n = I_{N-n+1}$ ($n = 1, 2, \dots, N$) for even number N . Value $\gamma = 0$ corresponds to the uniform distribution and $\gamma = 1$ determines illumination of the array aperture with magnitude I_n which decreases almost to zero from the center to the edge of the array. Table 2.1 presents the taper efficiency calculated with formulas (2.9) and (2.10) for different element numbers N .

The aperture efficiency value < 1 shortens communication range. However, reduced sidelobes increase the immunity to the interference sources. Therefore, antenna design engineer has to choose reasonable compromise between the sidelobes level and the gain loss to satisfy the communication system requirements.

2.3 Planar Array Factor

The array factor for the planar equally spaced array with N elements in each column and M elements in each row (Fig. 2.1b) is as in following [21]

$$AF_{\text{planar}}(\theta, \phi) = \sum_{n=1}^{n=N} \sum_{m=1}^{m=M} I_{nm} \cdot e^{j(\delta_{nm} + k \cdot d \cdot n \cdot \sin \theta \cdot \cos \phi + k \cdot d \cdot m \cdot \sin \theta \cdot \sin \phi)} \quad (2.11)$$

For uniform amplitude distribution ($I_{nm} = 1$) and equal phase distribution ($\delta_{nm} = 0$), the normalized planar array factor is defined as

$$\begin{aligned}
|AF_{\text{planar}}^{\text{norm}}(\theta, \phi)| &= \left| \frac{\sin\left(\frac{N}{2} \cdot k \cdot d \cdot \sin \theta \cdot \cos \phi\right)}{N \cdot \sin\left(\frac{k \cdot d \cdot \sin \theta \cdot \cos \phi}{2}\right)} \right| \cdot \left| \frac{\sin\left(\frac{M}{2} \cdot k \cdot d \cdot \sin \theta \cdot \sin \phi\right)}{M \cdot \sin\left(\frac{k \cdot d \cdot \sin \theta \cdot \sin \phi}{2}\right)} \right| \\
&= S_N(\alpha) \cdot S_M(\beta)
\end{aligned} \tag{2.12}$$

where the coordinates α and β are determined as $\sin \alpha = \sin \theta \cdot \cos \phi$, $\sin \beta = \sin \theta \cdot \sin \phi$ and

$$S_N(\alpha) = \left| \frac{\sin\left(\frac{N}{2} \cdot k \cdot d \cdot \sin \alpha\right)}{N \cdot \sin\left(\frac{k \cdot d \cdot \alpha}{2}\right)} \right|, \quad S_M(\beta) = \left| \frac{\sin\left(\frac{M}{2} \cdot k \cdot d \cdot \sin \beta\right)}{M \cdot \sin\left(\frac{k \cdot d \cdot \beta}{2}\right)} \right|; \tag{2.13}$$

The main lobe (principal maximum) and grating lobes of the terms $S_N(\alpha)$ and $S_M(\beta)$ are located at the angles (similar to the linear array) such that

$$\frac{d}{\lambda} \cdot \sin \alpha = \pm r_1; \quad \frac{d}{\lambda} \cdot \sin \beta = \pm r_2; \quad r_1 = 0, 1, 2, \dots; \quad r_2 = 0, 1, 2, \dots \tag{2.14}$$

Main lobe corresponds to $r_1 = 0$ ($\alpha = 0^\circ$) and $r_2 = 0$ ($\beta = 0^\circ$). To avoid grating lobes, the row and column spacing between the elements of the planar array has to be less than the wavelength. The beamwidth value of the main lobe between two adjacent nulls along the axis x can be determined from the expressions (2.5) and (2.6) by replacing θ with α and element spacing d with d_x . Similar logic can be used for estimating of the beamwidth value along the axis y by replacing θ with β and d with d_y . Formulas (2.13) present the pattern of planar array as the antenna pattern of two multiplicatively combined orthogonal linear arrays [22, 23]. These expressions show that the angular resolution of the planar array with N^2 elements in the main X or Y planes can be equivalent to the array consisting of two orthogonal linear arrays with total number of elements $2N$. More than 50 years ago, Mills [24] employed such technique (Mills Cross Technique) to achieve high angular resolution with a relatively small numbers of antennas.

Directivity for the planar array factor is expressed by a more complicated formula than Eq. (2.7) or (2.8). However, for the array with a large number of isotropic elements, directivity value can be estimated by the simple rough approximation [21]

$$D_{\text{planar}} \approx \pi \cdot D_{\text{linearx}} \cdot D_{\text{lineary}} \tag{2.15}$$

where D_{linearx} and D_{lineary} are the directivities of linear array factors along the x and y axes, respectively. For a planar array with half wave spacing along the x and y coordinates, directivity value is proportional to the total array element number $D \simeq \pi \cdot N \cdot M$. More accurate value [25, 26] directivity value for different element numbers, as a function of the element spacing are presented in Fig. 2.3b. Plots, like curves obtained for linear array, have dips caused by the emergence of

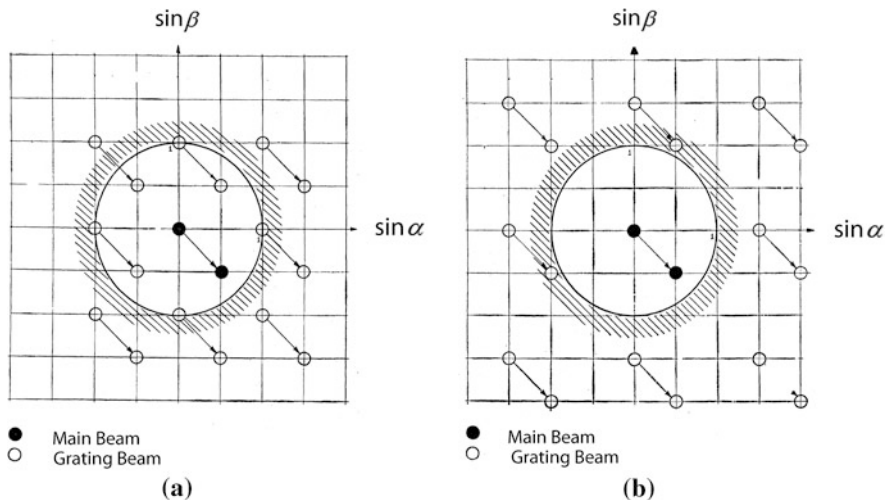


Fig. 2.5 Diagram showing grating beams: **a** Element spacing equal λ ; **b** Element spacing equal $2/3 \times \lambda$

grating lobes into the visible region when the element spacing is closed to the wavelength.

2.4 Array Factor for Circular Configuration

Referring to Fig. 2.1d, let us assume that N equally spaced isotropic elements are placed on x - y plane along a circular ring of radius a . The antenna factor can be expressed as [21]

$$AF_{\text{circular}} = \sum_{n=1}^N I_n \cdot e^{j(k \cdot a \cdot \sin \theta \cdot \cos(\phi - \phi_n) + \delta_n)} \quad (2.16)$$

where I_n = amplitude excitation of the n th element, $\phi_n = \frac{2 \cdot \pi \cdot n}{N}$ = n th angular position of element, δ_n = phase excitation of the n th array element. The maximum of the AF occurs when all the phase terms in (2.16) are equal

$$k \cdot a \cdot \sin \theta \cdot \cos(\phi - \phi_n) + \delta_n = 2 \cdot \pi \cdot r \quad r = 0, \pm 1, \pm 2, \dots \quad (2.17)$$

If $\delta_n = 0$ for all n numbers, the main maximum ($r = 0$) occurs for the angle direction $\theta = 0^\circ$

For uniform amplitude distribution ($I_n = 1$ for $n = 1, 2 \dots N$) expression (2.16) can be simplified as $AF_{\text{circular}} \approx N \cdot J_0(k \cdot \rho_0)$; where $J_0(x)$ = zero order Bessel function; $\rho_0 = a \cdot \sin \theta$. Typically, circular arrays are used in the smart antenna systems that provide adaptive beamforming to enable the formation (simultaneously or successively) of beam toward the desired signal angle direction and

nulls toward the angles of interfering signals. Uniformly circular antenna array can be electronically rotated in the plane of array without significant change of the beam shape, providing 360° azimuth coverage area [27].

2.5 Array Factor for Electronically Controlled Phased Arrays

2.5.1 Design with Analog Phase Shifters

Schematically, linear passive phase array with electronic beam control is presented in Fig. 1.7a. The linear system consists of N equally spaced identical isotropic elements. Each phase shifter has a special electrical control circuit, that can change the phase of the received signal. Let us assume that the space between the elements of the equally spaced linear antenna array is equal to d , and we want to receive a signal coming from the angle direction θ_0 . Assume that electronically controlled phased shifters provide a progressive phase shift between the adjacent antenna elements $\Delta\delta = \Delta\delta(\theta_0)$, then

$$\Delta\delta(\theta_0) = -k \cdot d \cdot \sin \theta_0; \delta_n = -k \cdot d \cdot n \cdot \sin \theta_0; \quad (2.18)$$

The linear antenna array factor (2.1) with uniform amplitude distribution can be expressed as

$$|AF_{\text{linear}}(\theta, \theta_0)| = \left| \frac{\sin\left(\frac{N}{2} \cdot k \cdot d \cdot (\sin \theta - \sin \theta_0)\right)}{\sin\left(\frac{k \cdot d \cdot (\sin \theta - \sin \theta_0)}{2}\right)} \right| \quad (2.19)$$

Equation (2.19) has a maximum value equal to N for the angle directions $\theta = \theta_r$,

$$\theta_r = \arcsin\left(\pm \frac{\lambda \cdot r}{d} + \sin \theta_0\right); \quad r = 0, 1, 2, \dots \quad (2.20)$$

$r = 0$ corresponds to the main beam angle position ($\theta = \theta_0$) and $r \neq 0$ determines the angle positions of the grating unwanted lobes.

As we can see from the expression (2.20), the closest unwanted grating lobe will be not appeared in visible space when

$$\frac{d}{\lambda} < \frac{1}{1 + \sin|\theta_0|} \quad (2.21)$$

Let us assume that that scanning angle range is equal $|\theta_0| < 60^\circ$. Expression (2.21) indicates that inter-element space d in this case is $< 0.53\lambda$. Therefore, to avoid grating lobes in scanning angle sector -60 to $+60$ degrees we have to choose an inter-element spacing of about 0.53λ , not more.

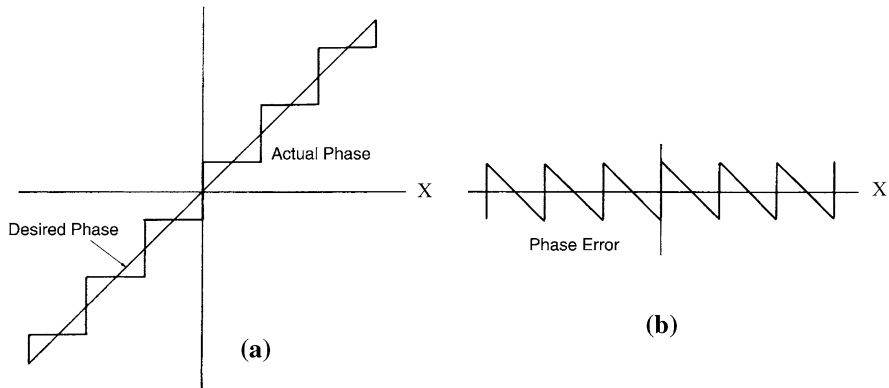


Fig. 2.6 **a** Phase shift for electronic scanning; **b** Phase error function

The absolute value of array factor for equally spaced planar array is given by

$$|AF_{\text{planar}}| = \left| \frac{\sin\left(\frac{N}{2} \cdot k \cdot d \cdot (\sin \alpha - \sin \alpha_0)\right)}{\sin\left(\frac{k \cdot d \cdot (\sin \alpha - \sin \alpha_0)}{2}\right)} \right| \cdot \left| \frac{\sin\left(\frac{M}{2} \cdot k \cdot d \cdot (\sin \beta - \sin \beta_0)\right)}{\sin\left(\frac{k \cdot d \cdot (\sin \beta - \sin \beta_0)}{2}\right)} \right| \quad (2.22)$$

Where $\sin \alpha = \sin \theta \cdot \cos \phi$; $\sin \alpha_0 = \sin \theta_0 \cdot \cos \phi_0$; $\sin \beta = \sin \theta \cdot \sin \phi$; $\sin \beta_0 = \sin \theta_0 \cdot \sin \phi_0$

To avoid grating lobes for scanning angles $\alpha_0 = \pm 60^\circ$ or $\beta_0 = \pm 60^\circ$ from broadside direction it is necessary to choose inter-space distances along x and y coordinates $< 0.53\lambda$.

Figure 2.5 presents the diagram which shows the number of grating beams in a visible range, depending on the scanning angle values α and β .

Figure 2.5a corresponds to the spacing between elements equal wavelength and Fig. 2.5b is obtained for spacing equal to two-thirds of wavelength. Equation (2.22) is an estimation of the radiation pattern with analog phase shifters that vary phases continuously from 0° to 360° . Such electronically controllable phase shifters are very expensive and typically are not used in practice.

2.5.2 System with Digital Phase Shifters

Most phase shifters are digitally controlled, so they realize phase shifts with a discrete Δ equal to $\Delta = \frac{2\pi}{2^q}$, where q is the number of bits, and 2^q is the number of digital phase shifter phase states. For example, a one-bit ($q=1$) digital phase shifter produces only two phases: 0° and 180° , a two-bit digital shifter can realize four phases $0, \pi/2, \pi, 3\pi/2$, and a three-bit digital phase shifter can realize phases:

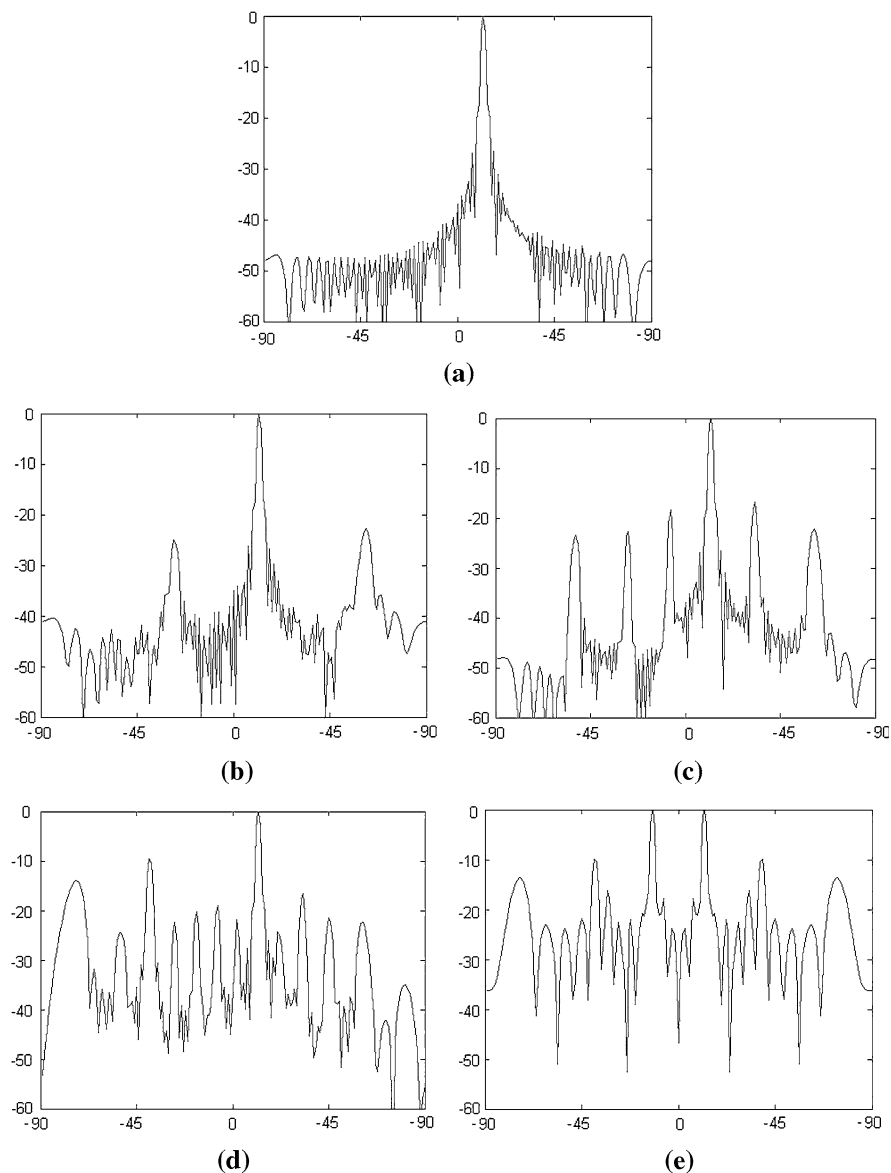


Fig. 2.7 Computer simulation of 64 element linear array with spacing $\lambda/2$, scan angle 12° : **a** Analog phase shifters; **b** $\Delta = 22.5^\circ$; **c** $\Delta = 45^\circ$; **d** $\Delta = 90^\circ$; **e** $\Delta = 180^\circ$

$0, \pi/4, \pi/2, 3\pi/4, \pi, 5\pi/4, 3\pi/2, 7\pi/4$. Figure 2.6a shows the ideal (desired) linear phase curve for electronic scanning as a function of the x coordinate (linear array is placed along this axis) and approximation (actual phase) caused by the stair-step phase. Phase error is demonstrated in Fig. 2.6b.

It is seen that the error between the ideal curve and its approximation is a periodic function of the X coordinate. Periodic errors cause main lobe attenuation, produce a set of lobes called as “quantization lobes”, and cause error in the main beam pointing position. It is known [28, 29] that the array factor for a linear antenna array with digital phase shifters can be presented as

$$AF_{\text{linear}}^{\text{digit}} = \sum_{m=-\infty}^{m=\infty} C_m \cdot \sum_{n=1}^N I_n \cdot e^{j \cdot (k \cdot d \cdot \sin \theta - k \cdot d \cdot (\sin \theta_0 + m \cdot \frac{2\pi}{\Delta}))} \quad (2.23)$$

where parasitic lobe coefficients C_m are given by

$$C_m = \frac{(-1)^m \cdot \sin(\frac{\Delta}{2})}{(\frac{\Delta}{2} - \pi \cdot m)} \quad (2.24)$$

Formula (2.23) shows that the array factor of the array with digital phase shifters is a sum of the linear array factors with amplitude weightings (2.24) and beam angle directions

$$\theta_{rm} = \arcsin\left(\frac{\lambda \cdot r}{d} + \left(1 + \frac{2 \cdot \pi}{\Delta} \cdot m\right) \cdot \sin \theta_0\right) \quad (2.25)$$

where $r, m = 0, \pm 1, \pm 2 \dots$ (any positive or negative integer numbers).

An array factor with $m = r = 0$ corresponds to the main beam while beams with number $m \neq 0$ determine unwanted (parasitic or quantization lobes) lobes. It is seen that the angle directions (2.25) depend on the scanning angle θ_0 , and the parasitic lobe amplitudes decrease with increasing number m . Simple estimation of the main beam loss effect due to digital phase shifters is

$$\Delta AF_{\text{linear}} \approx C_0 = \frac{\sin(\frac{\Delta}{2})}{\frac{\Delta}{2}} \quad (2.26)$$

Quantization lobe (QL) values depend only on the scanning angle position and do not depend on the array amplitude distribution. The maximum value of quantization lobe QL ($m = 1$) is equal [with respect to the main lobe (2.26)] to

$$QL \approx \left| \frac{C_1}{C_0} \right| = \frac{1}{\frac{2 \cdot \pi}{\Delta} - 1} \quad (2.27)$$

Figure 2.7 presents computer calculations of the linear array factor for the equally spaced ($d/\lambda=0.5$) elements ($N = 64$). Scan angle θ_0 from the normal to the array is equal to 12° , where normal to the array (direction z) corresponds to the angle 0° . Amplitude distribution provides sidelobe levels <-20 dB. Figure 2.7a presents the results for analog phase shifters, Fig. 2.7b–e show the array factor for the same antenna with digital phase shifters. As we can see, a linear array factor with one bit phase shifters leads to the being split beam into two equally main

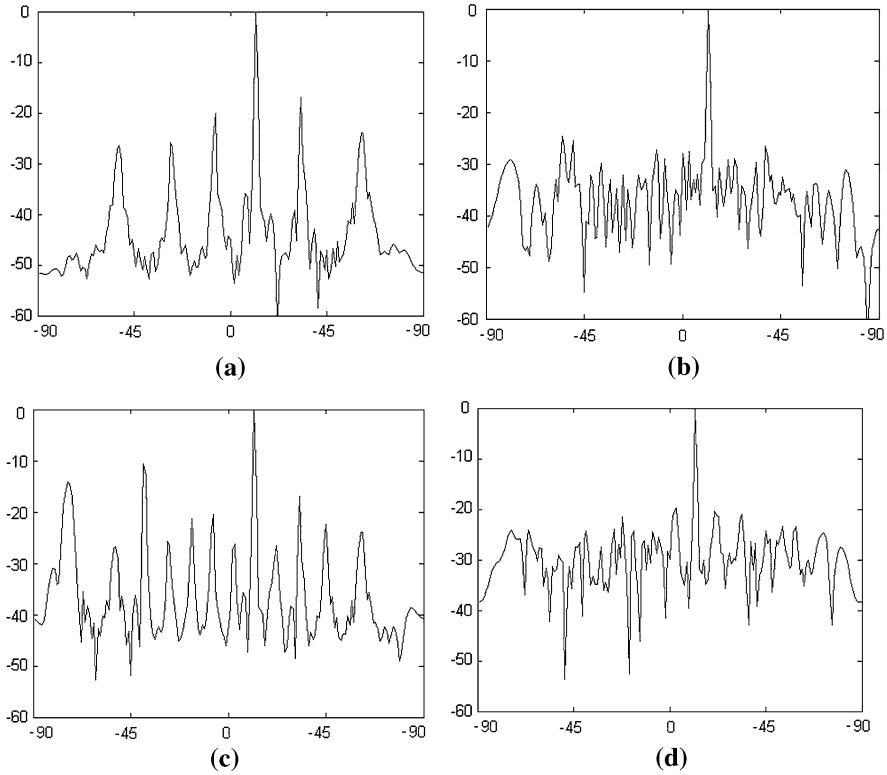


Fig. 2.8 Simulation results for 132 element linear array factor with randomizing periodic phase error: **a** Three-bit phase shifters without randomizing; **b** Three-bit phase shifters with randomizing; **c** Two-bit phase shifters without randomizing; **d** Two-bit phase shifters with randomizing

Table 2.2 Possible phase states for one bit phase shifters

| Element Number → | 1 | 2 | 3 | 4 | 5 | 6 | 7 | 8 |
|-------------------|-------|-------|-------|---|---|-------|-------|-------|
| Scan Angles ↓ | | | | | | | | |
| 1: 0°–9° | 0 | 0 | 0 | 0 | 0 | 0 | 0 | 0 |
| 2: 9°–12° | π | 0 | 0 | 0 | 0 | 0 | 0 | π |
| 3: 12°–20° | π | π | 0 | 0 | 0 | 0 | π | π |
| 4: 20°–26° | π | π | π | 0 | 0 | π | π | π |
| 5: 26°–37° | 0 | π | π | 0 | 0 | π | π | 0 |
| 6: 37°–46° | 0 | 0 | π | 0 | 0 | π | 0 | 0 |
| 7: 46°–60° | π | 0 | π | 0 | 0 | π | 0 | π |

lobes. The calculated values of the levels and angle positions of parasitic lobes approximately correspond to the estimations (2.24)–(2.27).

A few different methods [28–32] were offered to reduce these parasitic lobes. One of the simplest and effective methods can be realized using the feed network

Table 2.3 Average linear array factor parameters

| q (bit number) → | 2 | 3 | 4 | 5 |
|------------------------|-------|--------|--------|--------|
| $\delta\theta_0$ | 1.76 | 0.98 | 0.46 | 0.23 |
| SL_{\max} (dB) | -6.97 | -10.19 | -11.62 | -12.18 |
| D_{loss} (dB) | 0.82 | 0.2 | 0.047 | 0.012 |

shown in Fig. 1.7c, d. An antenna array with digital phase shifters is illuminated by a spherical wave with the phase difference between edge and central elements of about 360° . According to the known array geometry, it can calculate phase shifts required for converting spherical wave into a plane wave-front and to calculate linear phase shift along the array aperture for scanning beam toward the predetermined angle direction. In this case, the periodic error between the illuminated phase and the realized with digital phase shifters phase [32] is destroyed, and parasitic lobes are significantly reduced. Similar effect can be obtained if the illuminated wave is presented by quasi-random phase distribution along the array (for example, uniform random phase distribution in the range -180° – 180°). Such phase distribution can be produced by special feeding network design. Random phases required for the compensation of feeding network phases are stored in the computer memory and do not depend on the scan angle. Figure 2.8 demonstrates simulation results for the linear array factor of the antenna array consisting of 132 elements under condition that array phase error shown in Fig. 2.6a is destroyed using random phases, and a scan angle of 12° . Figure 2.8a, b demonstrate linear array factor with and without randomizing phase error for three-bit phase shifters, Fig. 2.8c, d show similar curves for two-bit phase shifters. As we can see, randomizing the periodic phase error significantly reduces the parasitic lobes, while increases the average power sidelobe level P_{average}

$$P_{\text{average}} \approx \frac{\Delta^2}{12 \cdot N} \quad (2.28)$$

This value is a rough estimation and usable for multi-element antenna array.

The error in the main beam pointing of the multi-element array can be estimated as [15]

$$\delta\theta \approx \frac{\Delta}{k \cdot d \cdot N \cdot \sqrt{N} \cdot \cos(\theta_0)} \quad (2.29)$$

Where θ_0 = scanning angle.

For small element arrays, the expression (2.28) has to be revised by computer simulations.

As an example, Table 2.2 [33] shows detailed phased distributions for the 8 element array with an inter-element space $\lambda/2$ and one bit digital phase shifters.

With one bit phase shifter, the phase is limited to two states: 0° and 180° . The maximum deviation from the phase that is required for the antenna element to steer

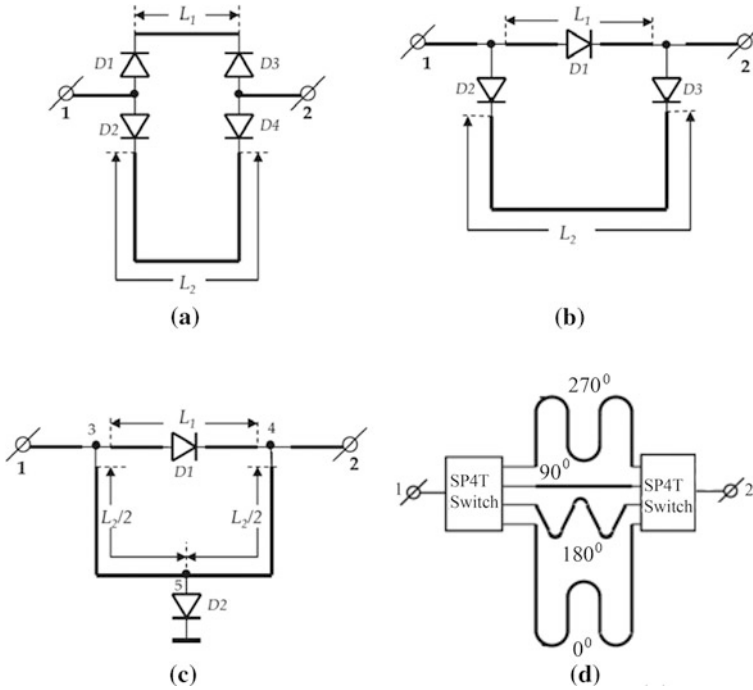


Fig. 2.9 Phase shifter circuit topology: **a–c** Transmission line design; **d** SP4T switch configuration

the beam is 90° . Only seven phase distributions are available to cover 60° scan range.

As we can see, all array elements are in phase for the scan angles from 0° to 9° , and there is no beam steering within this angle range. Note that the maximum power value cannot be reached for $\theta_0 > 9^\circ$ because of the presence of two main lobes symmetrically located with respect to the broadside direction.

A two-bit phase shifter ($q = 2$) provides four phase states within 0 – 360° phase range: 0° , 90° , 180° , and 270° . The maximum deviation required for each element to steer the beam is then 45° . The array factor value does not change for scan angles from 21° to 30° and from 30.5° to 40.5° .

A three-bit phase shifter ($q = 3$) gives eight possible phase states, starting from 0° to 45° . The maximum deviation of the phase of each element is then 22.5° . The beam pointing remains constant for the largest angular ranges: 43° – 49° and 49° – 55.5° .

A four-bit phase shifter corresponds to sixteen phase steps with a discrete equal to 22.5° . The maximum deviation of the phase is now 11.25° . Table 2.3 summarizes the average array factor parameters for the eight element array with two- to five-bit phase shifters. The average was realized by considering a scan angle varying from 0° to 60° with a 0.5° step. The scan angle deviation $\delta\theta_0$ is expressed in degrees, SL_{\max} is the maximum of sidelobe level, and D_{loss} is an average directivity loss.

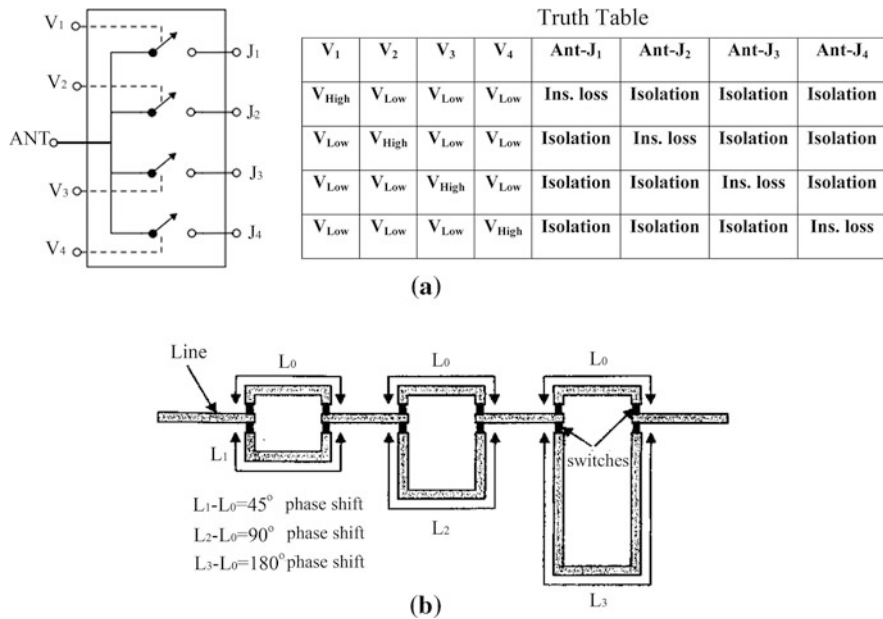


Fig. 2.10 **a** Truth table for SP4T switch; **b** Three—Bit switched line phase shifter

2.5.3 Pin Diode Digital Phase Shifter Topology

The phase of an electromagnetic wave is changed when propagating through the channel, which includes phase shifter device. The major parameters of a phase shifter are frequency range, bandwidth, total phase variance, insertion loss, and switching speed. The simplest phase shifter circuits based on transmission line design and pin diodes elements are presented in Fig. 2.9.

By switching the signal between two lines L1 and L2, it is possible to realize specific phase shift [34]:

$$\Delta\phi = \left(\frac{2 \cdot \pi \cdot (L2 - L1)}{\lambda} \right) \quad (2.30)$$

Switched line phase shifters generally are digital elements with a discrete $\Delta = \frac{2\pi}{2^q}$. For example, to get a 180° phase shift, the required physical length difference $\Delta L = L2 - L1$ should be $\lambda/2$, to provide a phase shift equal to 90°, it is necessary to have a physical length difference of $\lambda/4$, and for a 45° phase $\Delta L = \lambda/8$. Typically, digital phase shifters use PIN diodes as phase control elements due to their high speed switching time (a few microseconds) and relatively simple bias circuits. PIN diodes insertion losses are about 1–3 dB, depending of the frequency range. Commercially available pin diode switch assemblies are classified by the different numbers of outputs: SPST (one input, one output), SPDT (one input,

two outputs), SP3T (one input, three outputs) etc. Pin diode Truth Table shows controllable voltage values (High or Low) when connecting the input line with the output line to provide the desired phase shift. The block diagram example of a two bit phase shifter based on use of SP4T switch is demonstrated in Fig. 2.9d, and Truth Table for such switch is presented in Fig. 2.10a.

The control voltage V_{High} is equal 5 volts and V_{Low} is zero volts. The isolation corresponds to the losses of 30 dB and the insertion losses are <1.5 dB. Figure 2.10b shows a two-bit switched line phase shifter using SPDT integrated circuits. Many commercially pin diode switches are available on the market, for example, from Skyworks Solutions, RF Micro Devices, Avago Technologies, etc.

2.6 Antenna Array Performances

2.6.1 Array Element Radiation Pattern and Mutual Coupling

So far, we supposed that the array elements have omnidirectional radiation patterns. The elements in a real array are not isotropic or isolated sources. The array element radiation pattern [35] is determined as a pattern taken with a feed at a single element in the array, and all other elements are terminated by the matched loads. The pattern $F_{m \text{ element}}(\theta, \phi)$, called an “active element pattern”, is different from the isolated element pattern $F_{\text{element}}^{\text{isolated}}(\theta, \phi)$, which reveals the radiation pattern of the antenna element in free space without coupling from “neighbors”. An active element pattern depends on the position of the element in the array: patterns of edge elements differ from the center located antenna pattern.

The finite array coupling effects may produce increased sidelobes, main beam squint, shifted nulls, and array blindness in some scan angles. Therefore, it is very important to study the antenna array parameters, including mutual coupling effects. An active element radiation pattern surrounded by others elements can be described using coupling scattering coefficients S_{mn} [37]

$$F_{m \text{ element}}(\theta) = F_{\text{element}}^{\text{isolated}}(\theta) \cdot \left(C_{mm} \cdot e^{j \cdot k \cdot d \cdot (m-1) \cdot \sin \theta} + \sum_{n=1; n \neq m}^N S_{nm} \cdot e^{j \cdot k \cdot d \cdot (n-1) \cdot \sin \theta} \right) \quad (2.31)$$

Coefficient C_{mm} denotes the coupling from the array aperture to the output transmission line.

The active reflection coefficient seen at the m th, element is given as [38]

$$\Gamma_m(\theta) = e^{j \cdot k \cdot d \cdot (m-1) \cdot \sin \theta} \cdot \sum_{n=1}^N S_{mn} \cdot e^{-(n-1) \cdot k \cdot d \cdot \sin \theta} \quad (2.32)$$

Generally, $\Gamma(\theta) \neq \Gamma(-\theta)$, except of an infinite array of symmetric elements or for the central element of a finite array having an odd number of symmetric elements.

The results of the fundamental reference paper [35] shows that the gain of the active element pattern in the large array where end effects can be ignored is given by simple formula

$$G_{\text{element}}(\theta) = G_{\text{isolated}}(\theta) \cdot [1 - |\Gamma(\theta)|^2] \quad (2.33)$$

where $\Gamma(\theta) = \Gamma_m(\theta) = \Gamma_m(-\theta)$ ($m = 1, 2 \dots N$), $G_{\text{isolated}}(\theta)$ = gain of a single isolated element.

The upper limit (maximum) energy value received by the single element is proportional to the array element area. Furthermore, since the effective area of an element is proportional to its projected area $A = d_x \cdot d_y$ (d_x and d_y are element spacings along x and y axis) in the direction of interest, the gain should have a $\cos \theta$ variation with an angle

$$G_{\text{element}}^{\text{max}}(\theta) = \frac{4 \cdot \pi \cdot d_x \cdot d_y}{\lambda^2} \cdot \cos \theta \quad (2.34)$$

The active reflection coefficient $\Gamma_m(\theta_0)$ can be used to compute the active input impedance at the m th array element [38]

$$Z_{in}^m(\theta) = Z_0 \cdot \frac{1 + \Gamma_m(\theta)}{1 - \Gamma_m(\theta)} \quad (2.35)$$

where Z_0 = is the characteristic impedance of the transmission line with matched generator.

If the scanning angle is equal to zero, then

$$Z_{in}^m(0) = Z_0 \cdot \frac{1 + \sum_{n=1}^N S_{mn}}{1 - \sum_{n=1}^N S_{mn}} \quad (2.36)$$

The matrix $[S]$ for the scattering parameters and matrix $[Z]$ for the impedance parameters are related as [15]

$$[S] = \frac{[Z] - Z_0}{[Z] + Z_0} \quad (2.37)$$

Impedance matrix $[Z]$ contains all the inter-element mutual impedances Z_{mn} ; the mutual impedances, in principle, are calculated between two elements, with all the other elements open circuited. The mutual impedance between any two elements in the array is found by dividing the open-circuit voltage at one element by the current at the other element

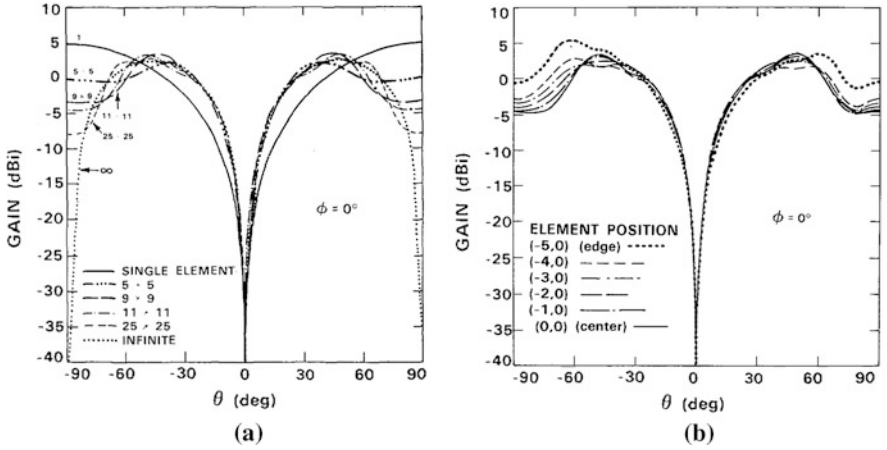


Fig. 2.11 **a** Radiation pattern simulation results for monopole element of planar array: Central element, different number of array elements; **b** Radiation pattern versus element position; [39] ©1985 IEEE

Table 2.4 Reactive impedance of central element versus array size

| No. rows # | No. columns | Total number of elements | Reactive portion |
|------------|-------------|--------------------------|------------------|
| 3 | 3 | 9 | +j5.9 |
| 5 | 5 | 25 | +j3.2 |
| 7 | 7 | 49 | +j2.4 |
| 9 | 9 | 81 | +j2.1 |
| 11 | 11 | 121 | +j2.0 |
| 25 | 25 | 625 | +j1.8 |

$$Z_{mn} = \frac{V_m}{I_n} \text{ for } I_m = 0 \tag{2.38}$$

For an array consisting of two elements, the relationships between mutual scattering components and mutual impedance components are given by

$$S_{12} = \frac{2 \cdot Z_{12}}{(Z_{11} + 1) \cdot (Z_{22} + 1) - Z_{12} \cdot Z_{21}} \tag{2.39}$$

$$S_{21} = \frac{2 \cdot Z_{21}}{(Z_{11} + 1) \cdot (Z_{22} + 1) - Z_{12} \cdot Z_{21}} \tag{2.40}$$

$$S_{11} = \frac{(Z_{11} - 1) \cdot (Z_{22} + 1) - Z_{12} \cdot Z_{21}}{(Z_{11} + 1) \cdot (Z_{22} + 1) - Z_{12} \cdot Z_{21}} \tag{2.41}$$

Table 2.5 Reactive impedance as a function of element location for 11×11 antenna array

| Element position | Imaginary impedance portion (ohms) |
|--------------------------------|------------------------------------|
| Center element (0,0) | +j2 |
| Edge element of the center row | +j7 |
| Corner element | +j12 |
| Isolated element (Reference) | +j21 |

Table 2.6 Amplitude of the coupling coefficient (dB scale) between central array element and element number n ($n = 1, 2, 5$)

| Element # | 1 | 2 | 3 | 4 | 5 |
|-------------------|-----|-----|-----|-----|-----|
| $ S_{0n} ^2$ (dB) | -10 | -22 | -32 | -38 | -43 |

$$S_{22} = \frac{(Z_{22} - 1) \cdot (Z_{11} + 1) - Z_{12} \cdot Z_{21}}{(Z_{11} + 1) \cdot (Z_{22} + 1) - Z_{12} \cdot Z_{21}} \quad (2.42)$$

If the antenna elements are reciprocal, then

$$S_{11} = S_{22} \text{ and } S_{12} = S_{21} \quad Z_{12} = Z_{21} \text{ and } Z_{11} = Z_{22} \quad (2.43)$$

Below, we present some simulation and experiment results for the “active radiation pattern” for the element that is surrounded by the other passively terminated elements.

We collect and summarize the results for two kinds of arrays: monopole systems which are good candidates for car applications because they can be easily mounted on the car roof, and microstrip patch arrays for communication between roadside base stations and the vehicle.

a) Monopole Antenna Array

Figure 2.11a [39, 40] demonstrates simulation results for the central element of the planar array with different number of the radiators.

An array consisting of the quarter wavelength monopole elements is placed on the infinite ground plane (xy plane shown in Fig. 2.1b), and the element spacing is equal to half of the wavelength. The monopoles are assumed electrically thin, with a wire radius of 0.001λ . The radiation pattern is simulated for the single isolated monopole and for the actively exited monopole surrounded by 50 ohm terminated monopoles. Results are presented for the E_θ radiation pattern component in elevation plane, ground plane has infinite size. For the planar array with 5 columns and 5 rows the principal peak occurs at $\theta = 38^\circ$, for the arrays 9×9 , 11×11 , and 25×25 peak element gain is close to $\theta = 50^\circ$. It is seen, that for 11×11 array the element radiation pattern has small differences when compared to the results obtained for the 25×25 array. It means that the coupling coefficients S_{mn} (expression (2.31)) become negligible for the distance between the elements of

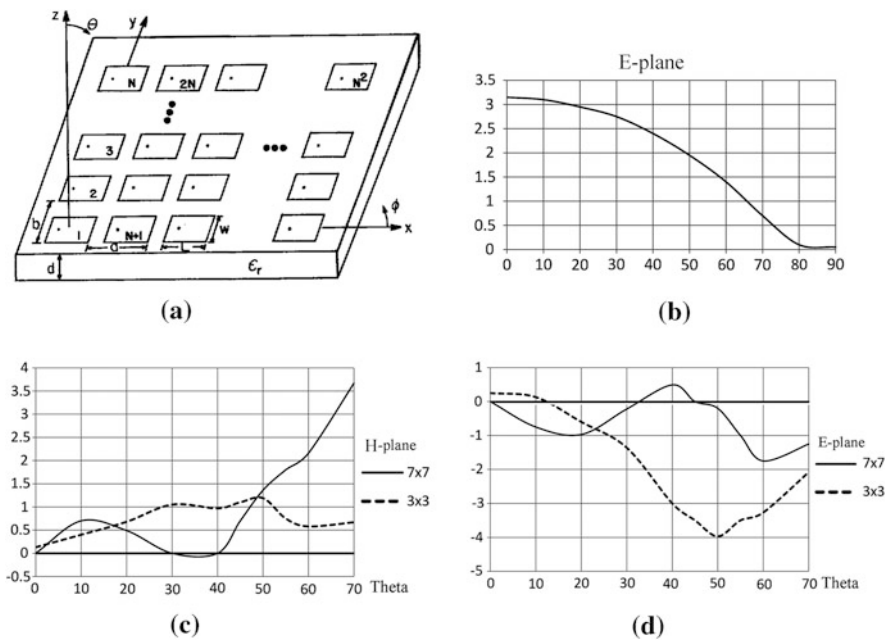


Fig. 2.12 **a** Rectangular patch array; **b** Radiation pattern of the central element in E-plane; **c**, **d** Variations of the radiation pattern of the central array element as a function of array element number

| Table 2.7 Coupling coefficient for microstrip array as a function of spacing between elements | | | | | |
|---|------|-----|------|-----|------|
| Spacing in wavelength | 0.25 | 0.5 | 0.75 | 1 | 1.25 |
| $ S_{12} ^2$ (dB) | −21 | −23 | −24 | −25 | −25 |

about seven wavelength. Also, the center element input impedance versus array size is summarized in Table 2.4. Input impedance for isolated $\lambda/4$ monopole is equal to $36 + j21$ Ohm. The real part of the input impedance of the active element is about 38 ohm and practically does not depend on the array size. However reactive impedance portion decreases when the number of array elements increases as shown in Table 2.4. So, impedance of the $\lambda/4$ monopole with $\lambda/2$ spacing tends to be purely resistive as the number of surrounding loaded monopoles increases, and the resistance is insensitive to the array size.

Figure 2.11b demonstrates the element pattern gain as a function of the element position along the center row of the 11 by 11 monopole array. Approximately, 2.2 dB of asymmetry occurs between the two (left and right) peaks of the edge element pattern. For monopoles, two or more elements away from the edge element, the pattern peak asymmetry is <0.5 dB. Table 2.5 shows the input impedance of a few elements of the 11×11 element array.

As it is seen, the imaginary part of the input impedance varies by <10 ohm. Calculations show that the real input impedance portion is relatively insensitive to element position in the 11×11 element array and is about 39 ohm.

Table 2.6 presents the experimentally measured coupling scattering parameters S for the central row elements in a planar antenna array (11×1 elements) operating at 1.3 GHz. Data are shown for the coupling coefficient $|S_{0n}|^2$ between the central active monopole marked as number 0 and n th element in row. The distance between the adjacent elements is about half of the wavelength.

As we can see, the coupling between adjacent elements is about -10 dB, while the coupling value between the central and fifth element is <-40 dB.

b) Rectangular Patch Array

It is known that microstrip antenna arrays [41–43] have found wide application for communication between the roadside base stations and the car antenna due to its several advantages, such as low profile, light weight, and low cost, etc.

Figure 2.12a shows an example of the microstrip finite antenna array model that is used to estimate the radiation pattern for the array element surrounded by a number of terminated to 50 ohm identical radiators. The operating frequency is 1.41 GHz, $W = 10.6$ cm, $L = 6.55$ cm, $d = 0.16$ cm, spacing between elements is equal to $0.5 \cdot \lambda_0$, λ_0 =wavelength in free space, dielectric constant is equal to 2.55. Presented data give an idea of how the mutual coupling coefficient depends on the distance between the adjacent microstrip elements.

Figure 2.12b presents central “active” element gain in the E-plane for the infinite array. The radiation pattern in the H-plane is slightly different from the curve demonstrated in Fig. 2.12b. Figure 2.12c, d show active element gain variations (dB scale) in E and H planes for central element in the passively loaded 50 ohm rectangular patch array schematically shown in Fig. 2.12a. Data are calculated based on the reference paper [41]. Solid horizontal line corresponds to the infinite array. Table 2.7 demonstrates the experimental data of the mutual coupling coefficient $|S_{12}|^2$ (dB scale) between two adjacent elements as a function of the distance S for the array shown in Fig. 2.12a.

2.6.2 Array Radiation Pattern

If the equally spaced array consists of a large number of antenna radiators, most of the elements “see” the uniform neighboring environment, and $F_{n \text{ element}}(\theta, \phi)$ can be approximated by an equal for all elements array radiation pattern $F_{n \text{ element}}(\theta, \phi) = F_{\text{element}}(\theta, \phi)$. In this case, fully excited array radiation pattern can be expressed as the product of the active element radiation pattern and the array factor

$$F_{\text{array}}(\theta, \phi) = F_{\text{element}}(\theta, \phi) \cdot AF_{\text{array}}(\theta, \phi) \quad (2.44)$$

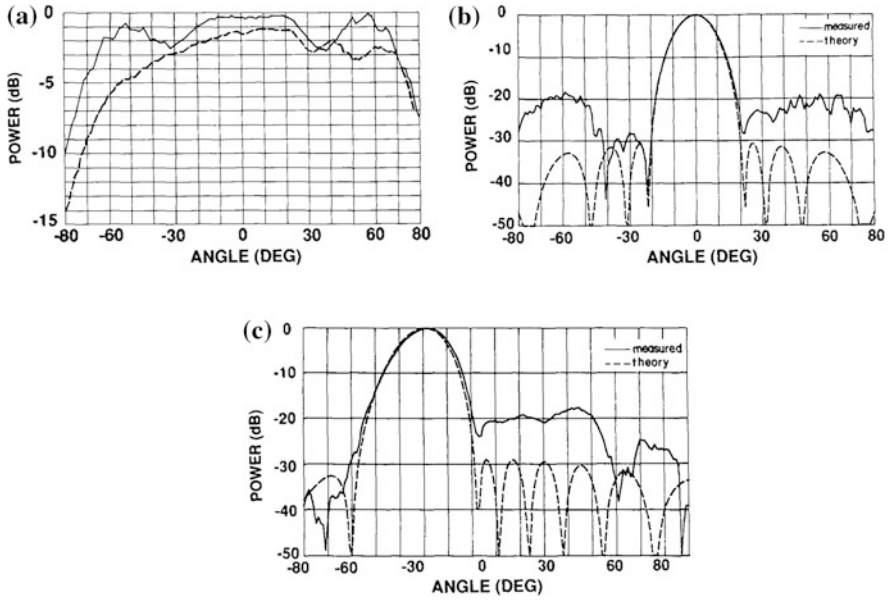


Fig. 2.13 **a** Radiation pattern of central (*solid line*) and edge (*dashed line*) elements of the linear waveguide X-band array; **b** Synthesized 30 dB Chebyshev array radiation patterns without mutual coupling (*theory-dashed line*) and measured with mutual coupling (*solid line*); **c** Radiation pattern for scan angle -30° without mutual coupling (*theory-dashed line*) and measured with mutual coupling (*solid line*)

where $AF_{\text{array}}(\theta, \phi)$ =antenna factor related to the linear or planar array. This well-known [15, 21] multiplication formula determines the array radiation pattern as a product of the element radiation pattern and the array factor. Strictly speaking, this formula is valid for infinite equally spaced array. For an ideally matched array with the element gain, which is given by the ratio (2.34), the maximum array gain toward the scanned angles θ_0 and ϕ_0 is given by

$$G_{\text{array}}^{\max}(\theta_0) = \frac{4 \cdot \pi \cdot d_x \cdot d_y}{\lambda^2} \cdot N \cdot \cos \theta_0 \quad (2.45)$$

This is the fundamental upper gain limit for the antenna array with a large number of elements when majority of elements sees the same “neighbors” [36]. Due to the reflection losses $\Gamma(\theta, \phi)$, the realized large array gain when scanning the beam toward the angle θ_0 is given [35]

$$G_{\text{array}}(\theta_0, \phi_0) = \frac{4 \cdot \pi \cdot d_x \cdot d_y}{\lambda^2} \cdot N \cdot \left(1 - |\Gamma(\theta_0, \phi_0)|^2\right) \cdot \cos \theta_0 \quad (2.46)$$

Formula (2.46) assumes identical reflections at each antenna element and does not take into consideration active losses in the feeding network and antenna elements. The gain of a fully excited linear array for $\theta = \theta_0$ and non-identical elements is [35]

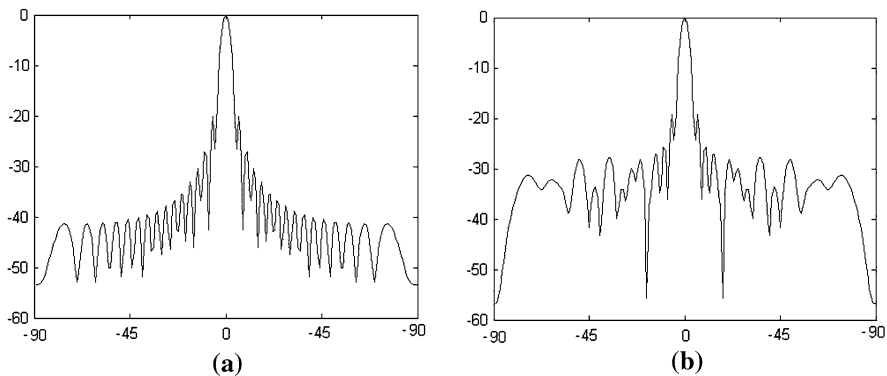


Fig. 2.14 Simulated radiation patterns for 32 element array with ideal element radiation pattern ($\cos \theta$): **a** Reference pattern with feeding network providing -28 dB sidelobes; **b** Pattern with phase and amplitude errors

$$G_{\text{array}}(\theta_0) = G_{\text{isolated}}(\theta_0) \cdot \left[N - \frac{\left| \sum_{n=1}^N \Gamma_n(\theta_0) \right|^2}{N} \right] \quad (2.47)$$

Mutual coupling is especially pertinent problem [37, 44] when the number of antenna elements is small, often precluding the use of conventional beam synthesis techniques (Chebyshev, Taylor, Bayliss, etc.). Inter-element coupling usually manifests by increased main beamwidth, filling nulls, and raised sidelobes levels. Small arrays are the main candidates for compact automotive applications, and, therefore, estimation of the array radiation pattern with a small element number is very important. Figure 2.13 shows simulation and measurement results for the linear array of X-band rectangular waveguides in the ground plane [37] with mutual coupling between antenna elements. Each element was in turn a column of 8 rectangular waveguides in a common H-plane, combined via a fixed 1:8 power divider.

The array axis, thus, was parallel to the E-plane and in this plane, the element spacing $d = 1.25 \text{ cm} = 0.517 \lambda$. The isolated element pattern corresponds to a normalized uniform aperture distribution

$$F_{\text{elemnt}}^{\text{isolated}}(\theta) = \frac{\sin\left(\frac{k \cdot l \cdot \sin \theta}{2}\right)}{\frac{k \cdot l \cdot \sin \theta}{2}} \quad (2.48)$$

where $l = 10.2 \text{ mm} = 0.417 \lambda$. Examples of the element patterns for a central and an edge element are shown in Fig. 2.13a. Figure 2.13b demonstrates synthesized 30 dB Chebyshev patterns obtained with and without the mutual coupling. The radiation pattern, calculated according to the multiplication formula (2.44) is presented by a dashed line, where the radiation pattern of the single element is simulated by formula (2.48). A solid line curve is the array pattern in the E-plane

with coupling effect. Figure 2.13c shows two radiation patterns for the scanning angle equal -30° : theory calculation without mutual coupling and measurement result obtained with coupling effect, which leads to the increasing of the sidelobe by approximately 10 dB.

Similar distortions of the array radiation pattern occur for the amplitude and phase errors due to the array element tolerances. Let us assume that the amplitudes and phases of the array elements have quasi-random errors due to the manufacturing process, and the antenna array consists of a large number of the elements. In such a situation, errors lead to: directivity (gain) reduction; raising of the average sidelobe level and of some individual sidelobes; errors in the main beam pointing and perhaps shape changing. The ratio of the gain obtained with errors to the gain without amplitude and phase distortions and an approximate average sidelobe level for multi-element array can be estimated as

$$\text{Gain loss} \approx e^{-\sigma^2} \approx \frac{1}{1 + \sigma^2}, \text{ Average Lidelobe Level} \approx \frac{\sigma^2}{N} \quad (2.49)$$

where $\sigma^2 = \sigma_a^2 + \sigma_\phi^2$, σ_a and σ_ϕ amplitude and phase standard deviations, respectively.

For a uniform square planar array of N elements per side, the standard deviation of the beam pointing error, in terms of the 3 dB beamwidth is [15]

$$\sigma_\theta \approx \frac{0.66 \cdot \sigma}{N} \quad (2.50)$$

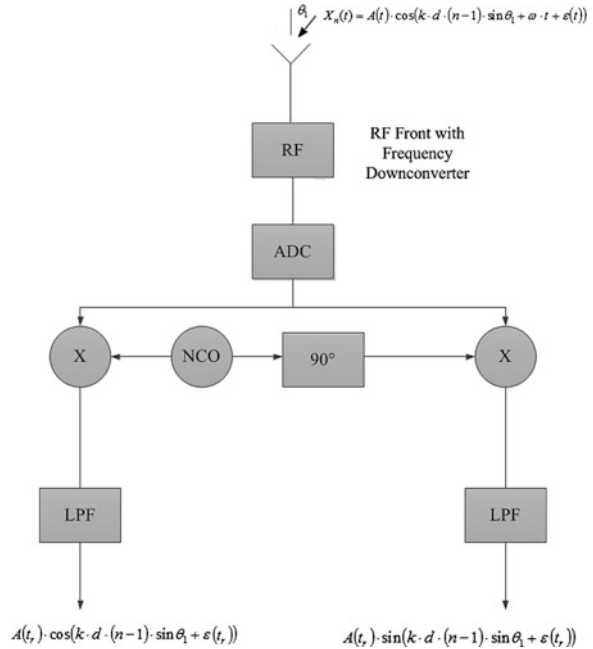
Figure 2.14 illustrates two radiation patterns for a 32 element linear array with ideal elements (element pattern is $\cos \theta$): the first one is the reference and it is obtained with a feeding network providing -28 dB sidelobes, while the second radiation pattern is a quasi-random realization of the radiation pattern with phase and amplitude errors ($\sigma_a = 0.1$, $\sigma_\phi = 15^\circ$).

According to the expressions (2.48) and (2.49) expected gain losses are about -0.2 dB, and the average sidelobe level is equal to -28 dB. It is necessary to note that formulas (2.49) and (2.50) present average estimations while different quasi-random realizations of amplitude and phase errors lead to quasi-random radiation pattern parameters.

2.7 Digital Beamforming

In digital beamforming (DBF), the operations of phase shifting, amplitude tapering for each element, and forming of the radiation pattern are produced digitally. From a technological point of view DBF is applicable for both the transmitting and receiving modes. However, for the transmitting mode, beam shape control and pattern nulling are not so critical. For the receiving mode, the main advantages of DBF are as follows:

Fig. 2.15 Simplified block diagram of digital array element, produces two quadrature components



- Multibeam operation which aims to scan wide angle sector with a few narrow beams simultaneously
- Flexible, accurate, and adaptive pattern shaping, including nulling toward the angle direction of the interference sources and synthesizing of the antenna pattern with extremely low sidelobe level
- High resolution techniques, which aim to resolve sources with closer angular spacing than one beamwidth
- Array element radiation pattern correction, which is important for small antenna arrays due to the mutual coupling effects

In this section, we show how to implement basic digital radiation pattern and estimate its main parameters.

In digital antenna array (DAA) system [45], the received signals are digitized at the element level. Since microwave frequency is too high to be directly digitized, each DBF receiver shifts the RF signal frequency down to the low intermediate carrier frequency, and then the low intermediate frequency signal is digitized with an analog to digital (A/D) converter. After the antenna signal has been successfully sampled in the digital domain, the signal needs to be processed by a digital down converter (DDC). DDC multiplies the digital signal with a sinusoidal signal and a 90° phase shifted version of the sinusoidal signal, both are generated by a local numerical controlled oscillator (NCO). Finally, both quadrature digital signals are filtered to suppress the intermediate frequency, creating two zero baseband quadrature signals. Figure 1.8d shows a simplified block diagram of the digital

antenna array. Each receiving element of this array shown in Fig. 2.15 has RF front-end with a low noise amplifier and a frequency down convertor, which shifts the signal frequency band to baseband. Analog to digital convertor (ADC), digitizes the baseband signal, and the circuit including numerically controlled oscillator (NCO) produces two quadrature components of the digitized signal that pass through low pass filters (LPF). Let us assume that a plane wave from angle direction θ_1 arrives at the element number n . This RF signal with a carrier frequency ω is modulated with slow time variable amplitude $A(t)$ and phase $\varepsilon(t)$. The circuit shown in Fig. 2.15 produces two quadrature digitized samples at a discrete time t_r ; $I_n(t_r) = A(t_r) \cdot \cos(k \cdot d \cdot (n-1) \cdot \sin \theta_1 + \varepsilon(t_r))$ and $Q_n(t_r) = A(t_r) \cdot \sin(k \cdot d \cdot (n-1) \cdot \sin \theta_1 + \varepsilon(t_r))$.

This information, taken for all array elements, determines the amplitude and phase distribution across the array elements due to the wave impinging on the array from the angle direction θ_1 . The digital beam processor forms an antenna array radiation pattern similar to the radiation pattern obtained with the electronically controlled phase array. Let us present the output digital signal in complex form (instead of two quadrature signals)

$$S_n(t_r, \theta_1) = I_n(t_r) + j \cdot Q_n(t_r) = A(t_r) \cdot e^{j \cdot k \cdot d \cdot (n-1) \cdot \sin \theta_1 + j \cdot \varepsilon(t_r)} \quad (2.51)$$

Without loss of generality we assume below that the incoming signal is a plane nonmodulated wave, i.e. $A(t_r) \equiv A$; $\varepsilon(t_r) \equiv \varepsilon$; $S_n(t_r, \theta) \equiv S_n(\theta)$. The beamforming processor multiplies the digital codes (2.51) by weighting the coefficients corresponding to some angle direction θ_0 . The array factor for (DAA) is determined by:

$$|AF_{\text{DAA}}(\theta_0)| = \left| \sum_{n=1}^N S_n(\theta_1) \cdot W_n^*(\theta_0) \right| \quad (2.52)$$

where: $W_n(\theta_0) = \text{Re}W_n(\theta_0) + j \cdot \text{Im}W_n(\theta_0)$ = complex weighting coefficients stored in the computer for a number of angles θ_0 .

$$W_n = e^{j \cdot k \cdot d \cdot (n-1) \cdot \sin \theta_0} \quad (2.53)$$

Using (2.52) and (2.53), the absolute DAA factor is given by

$$|AF_{\text{DAA}}(\theta_0)| = A \cdot \left| \frac{\sin\left(\frac{N}{2} \cdot k \cdot d \cdot (\sin \theta_1 - \sin \theta_0)\right)}{\sin\left(\frac{k \cdot d}{2} \cdot (\sin \theta_1 - \sin \theta_0)\right)} \right| \quad (2.54)$$

The radiation pattern in a digital array can be “scanned” by calculating of the expression (2.54) for different angles θ_0 , which are determined by weight coefficients W_n stored in the computer. The process of the radiation pattern calculation is named space beamforming. The beamformer can be implemented by using the Fast Fourier transform (FFT).

This expression is identical to the linear array factor (2.19) obtained for the electronically controllable phase array. If the number of the signal sources with amplitudes is more than one, for example L , and their amplitudes and phases are A_l

and ε_l , respectively, and the angle distance between them is more than the beamwidth of the antenna factor [see expression (2.5)], the array power factor can be expressed as

$$PF_{\text{DAA}} \approx \sum_{l=1}^L A_l^2 \cdot \frac{\sin^2\left(\frac{k \cdot d \cdot N \cdot (\sin \theta_l - \sin \theta_0)}{2}\right)}{\sin^2\left(\frac{k \cdot d \cdot (\sin \theta_l - \sin \theta_0)}{2}\right)} \quad (2.55)$$

Therefore, when the sources are separated from each other by the angle exceeding the array beamwidth function, (2.55) exhibits L distinguish peaks, with each peak being located at a point determined by the angle direction of the corresponding source.

To obtain good performance, the phase difference between the quadrature channels should not deviate significantly from 90° . The ADC is a critical element since it limits the system bandwidth and dynamic range. The output of an ADC has 2^R levels, where R = number of converter ADC bits. For example, an ADC with 10-bit output represent 1,024 (2^{10}) signal levels. That means that over the dynamic range from 0 % to 100 %, there will be 1,024 output binary numbers. The bit that represents the smallest voltage change is called the least significant bit. The number of effective bits is limited by the noise floor of the system. The maximum signal to noise ratio SNR and the number of effective bits are related as in [46]

$$\text{SNR} = \text{Number of Effective Bits} \cdot 6.02 + 1.76 \quad (2.56)$$

SNR is expressed in dB scale.

The other important ADC parameters are bandwidth and sampling rate. Bandwidth describes the frequency range in which the input signal can pass through the analog section of the ADC with minimal amplitude loss. It is recommended that the bandwidth of the digitizer be 3 to 5 times the highest frequency component of interest in the measured signal with minimal amplitude error [47]. The theoretical amplitude error of a measured signal is calculated from the ratio of the digitizer's bandwidth in relation to the input signal frequency f_{input}

$$\text{Error}(\%) = \left(1 - \frac{\text{ratio}}{\sqrt{1 + \text{ratio}}}\right) \cdot 100 \quad (2.57)$$

where $\text{ratio} = \frac{\text{bandwidth}}{f_{\text{input}}}$.

The sampling rate has to be greater than the theoretical Nyquist rate. The Nyquist theorem states that to avoid aliasing, a signal must be sampled at a rate greater than twice the highest frequency component of the signal to reconstruct the waveform accurately. However, to digitize the incoming signal, the digitizer's real-time sample rate should be at least three to four times the digitizer's bandwidth [48].

In addition, it is necessary to note that for proper operation of digital beamformer processor, the ADCs of all array elements have to convert analog signals to digital codes synchronically, otherwise the digital outputs will produce amplitude

and phase errors and eventually distort the computed antenna array factor [49]. The calibration of an ADC [50] is a key initial step in the successful application of algorithms reliant on spatial relationships across a multiple-antenna system.

References

1. Thiel A et al (2010) In situ vehicular antenna integration and design aspects for vehicle to vehicle communications, antennas and propagation (EuCap). In: Proceedings in the Fourth European Conference on 12–16 April 2010
2. Schack M et al (2010) Analysis of channel parameters for different antenna configurations in vehicular environments. Vehicular Technology Conference, IEEE, 2010
3. Sugiura S, Iizuka H (2007) Reactively steered ring antenna array for automotive application. IEEE Trans Antennas Propag, V 55(7):1902–1908
4. Song H et al (2002) Diversity antenna studies at 2.3 GHz for automotive applications, and MEMS-based antenna diversity switching circuit. In: Proceedings VTC 2002-Fall, 2002 IEEE 56th Vehicular Technology Conference, 2002
5. Nakano H et al (2010) Array antenna composed of bent four leaf elements. 3rd european conference on antennas and propagation EuCAP 2009
6. Rabinovich V et al (2010) Automotive antenna design and applications. CRC Press, Boca Raton
7. Nakanishi T et al (2006) Multiple-loop array antenna with switched beam for short range radars. Vehicular Technology Conference, 2006 VTC-2006 Fall, 2006 64th, 25–28 Sept 2006
8. Chen Z, Luk K (2009) Antennas for base stations in wireless communications. McGraw-Hill, New York
9. Choi B et al (2009) Circularly polarized H-shaped microstrip array antenna with T-slot for DSRC system roadside equipment. Microwave Opt Technol Lett, 51(6):1545–1548
10. Song C et al (2005) Compact low cost dual polarized adaptive planar phased Array for WLAN, IEEE Trans Antennas Propag 53(8):2406–2415
11. Mase K et al (2008) Performance evaluation of roadside to vehicle communication system using narrow antenna beam switching based on traffic flow model. GLOBECOM, Workshops
12. Song H et al (2002) Diversity antenna studies at 2.3 GHz for automotive applications, and mems-based antenna diversity switching circuit. In: Proceedings VTS 2002-Fall, IEEE 56th Vehicular Technology Conference pp 1096–1099
13. Khaleghi A et al (2005) Diversity techniques with dipole antennas in indoor multipath propagation. In: IEEE 16th international symposium on personal, indoor and mobile radio communication pp 669–673
14. Monzingo RA, Miller TW (2005) Introduction to adaptive arrays, SciTech Publishing
15. Robert C Hansen (2009) Phased array antennas, 2nd edn. Wiley, New York
16. Shen W et al (2007) A compact high performance linear series-fed printed circuit antenna array. In: ICMMT-07, International conference on Microwave and Millimeter Wave Technology
17. Lin C et al (2010) A compact linearly polarized antenna array with low sidelobe. In: International Conference on Microwave and Millimeter Wave Technology (ICMMT) pp 384–387
18. Gruszczynski S et al (2006) Reduced sidelobe four-beam n element antenna arrays by 4N butler matrixes. IEEE Antennas Wirel Propag Lett 2:430–434
19. Hancan RC (1985) Aperture efficiency of villeneuve \bar{n} arrays. IEEE Antennas Propag 33(6):666–669
20. Randy L (2010) Haupt antenna arrays: a computational approach. Wiley, New York
21. Balanis C (1997) Antenna theory analysis and design, 2nd edn. Wiley, New York

22. MacPhie R (2007) A millimeter wave multiplicative array with the power pattern of a conventional planar array. In: Antennas and propagation society international symposium, IEEE, pp 5961–5964
23. Aumann HM (2010) A pattern synthesis technique for multiplicative arrays. In: PIERs Proceedings, Cambridge, USA pp 864–867
24. Mills B, et al (1985) A high resolution radio telescope for use at 3.5 m. In: Proceedings of the IRE, pp 67–84
25. Forman BJ (1972) Directivity characteristics of scannable planar arrays. IEEE Trans Antennas Propag 20(3):245–252
26. Lee M et al (2000) Evaluation of directivity for planar antenna arrays. IEEE Antennas Propag Mag 42(3):64–67
27. Ioannides P, Balanis C (2005) Uniform circular and rectangular arrays for adaptive beamforming applications. IEEE Antennas Wirel Propag Lett 4:351–354
28. Rabinovich V (1975) Statistics of the array with digital phase shifters. J Commun Technol Electron (in Russia) 4:708–714
29. Smith M, Guo Y (1983) A comparison of methods for randomizing phase quantization errors in phased arrays. IEEE Trans Antennas Propag 31(6):821–828
30. Taheri S, Farzaneh F (2006) New methods of reducing the phase quantization error effects on beam pointing and parasitic side lobe level of the phased array antennas. Microwave Conference APMC 2006. Asia Pacific, pp 2114–2117
31. Guo Y et al (2003) Comparison of random phasing methods for reducing beam pointing errors in phased array. IEEE Trans Antennas Propag 51(4):782–787
32. Aronov FA (1966) New method of phasing for phased array using digital phase shifters. Radio Eng Electron Phys 11:1035–1040
33. Clenet M, Morin G (2003) Visualization of radiation-pattern characteristics of phased arrays using digital phase shifters. IEEE Antennas Propag Mag 45(2):20–35
34. Maloratsky L (2010) Electrically tunable switched line diode phase shifters. High Frequency Electronics 9(4):part1, 9(5):part2
35. Pozar D (1994) The active element pattern. IEEE Trans Antennas Propag 42(8):1176–1178
36. Hannan P (1964) The element gain paradox for a phased array antenna. IEEE Trans Antennas Propag 12(4):423–433
37. Steyskal H, Herd J (1990) Mutual coupling compensation in small array antennas. IEEE Trans Propag 38(12):1971–1975
38. Pozar D (2003) A relation between the active input impedance and the active element antenna pattern of phased array. IEEE Trans Antennas Propag 51(9):2486–2489
39. Fenn A (1985) Theoretical and experimental study of monopole phased array antennas. IEEE Trans Antennas Propag 33(10):1118–1126
40. Fenn A, Willwerth F (1984) Mutual coupling in monopole phased arrays. In: Antennas and Propagation Society Symposium 22:875–878
41. Pozar D (1986) Finite phased arrays of rectangular microstrip patches. IEEE Trans Antennas Propag 34(5):658–665
42. Jedlicka R et al (1981) Measured mutual coupling between microstrip antennas. IEEE Trans Antennas Propag 29(1):147–149
43. Pozar D (1981) Input impedance and mutual coupling of rectangular microstrip antennas. IEEE Trans Antennas Propag 30(6):1191–1196
44. Borowiec R et al (2002) Compensation of mutual coupling in small antenna arrays. In: International conference microwave, radars and wireless communication pp 894–897
45. Steyskal H (1987) Digital beamforming antennas: An introduction. Microwave J. 30(1):107–124
46. Tran T (2010) High speed DSP and analog system design, Springer Chapter 7
47. Bandwidth, Sample Rate, and Nyquist Theorem. NI Developer Zone - National Instrument www.ni.com/white-paper/2709/en
48. Top 10, Things to Consider When Selecting a Digitizer/Oscilloscope. NI Developer Zone - National Instrument www.ni.com/white-paper/4333/en

49. Bratchikov A, Dobycina E (2009) Digital antenna array calibration. In: 19th International crimean conference microwave and telecommunication technology, pp 401–402
50. Tyler N, Allen B, Aghvami H (2004) Adaptive antennas: the calibration problem. Commun Mag IEEE 42(12) pp 114–122

Antenna Arrays and Automotive Applications

Rabinovich, V.; Alexandrov, N.

2013, XVI, 192 p., Hardcover

ISBN: 978-1-4614-1073-7